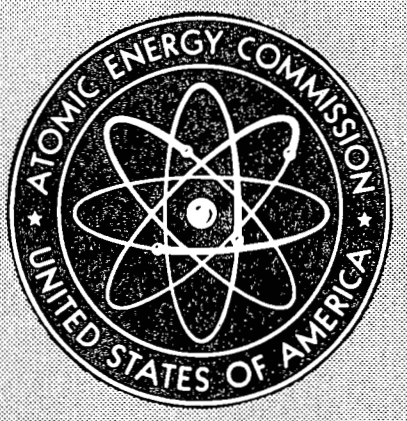

GEAP-3646

CALCULATION OF DOPPLER COEFFICIENT AND OTHER SAFETY PARAMETERS FOR A LARGE FAST OXIDE REACTOR

By
P. Greebler
B. A. Hutchins
J. R. Sueoka

March 23, 1961

Atomic Power Equipment Department
General Electric Department
San Jose, California

UNITED STATES ATOMIC ENERGY COMMISSION • OFFICE OF TECHNICAL INFORMATION

DISCLAIMER

GEAP-3646
REACTOR TECHNOLOGY

CALCULATION OF DOPPLER COEFFICIENT AND OTHER SAFETY PARAMETERS FOR A LARGE FAST OXIDE REACTOR

March 23, 1961

by

P. Greebler
B. A. Hutchins
J. R. Sueoka

Atomic Power Equipment Department
General Electric Company

Prepared Under
Contract AT(04-3)-189 PA#10
for the USAEC
San Francisco Operations Office

TABLE OF CONTENTS

TABLES AND FIGURES

CALCULATION OF DOPPLER COEFFICIENT AND OTHER SAFETY PARAMETERS FOR A LARGE FAST OXIDE REACTOR

CONCLUSIONS

The negative Doppler temperature coefficient of reactivity for a large fast oxide reactor is 5 to 10 times greater than that estimated for a small fast breeder such as FERMI I. The positive contribution to the Doppler coefficient by the Pu-239 was appreciable, indicating that this may be a safety problem for a small fast reactor containing a high atom ratio of Pu-239 to U-238. The sodium temperature coefficient is positive but sufficiently smaller in magnitude than the Doppler coefficient for optimum cases, so that power regulation should not be a problem. Reactivity insertion in a total loss of coolant accident appears to be the major control factor on the core size and composition.

Fuel slump does not constitute a major safety hazard in a large fast oxide reactor utilizing high density oxide (> 90% theoretical); however, reactivity effects of a more serious meltdown involving the entire core structure have not been evaluated. A beryllium reflector between the core and radial blanket of a large fast oxide reactor produced less than a two-fold increase in the neutron lifetime; only a very small safety advantage for the increased cost and design complexity.

Preliminary kinetics calculations indicate that the excess operating reactivity can safely be of the order of one and one-half to two dollars, which permits about a three month refueling cycle for fuel specific power of 1000 kw/kg Pu-239. Maintaining a large Doppler coefficient while simultaneously holding down reactivity insertion due to both total coolant loss and excess operating reactivity can best be accomplished at low sodium volume fractions. There is a similar incentive for holding the steel content to a minimum.

I INTRODUCTION

A large fast reactor fueled with plutonium and uranium oxides possesses several features which make it attractive for central power station applications. These include; (1) a high internal breeding ratio which facilitates attainment of high fuel burnup and increases the refueling interval for a given excess operating reactivity, and (2) a relatively low Pu-239 enrichment, permitting high fuel specific power. Obtaining a design which will inherently terminate a prompt critical power excursion is a major safety problem for a fast reactor.

In this respect an important advantage of a large oxide-fueled core over a metal-fueled core is the appreciable negative Doppler temperature coefficient of reactivity realized as a result of the degradation of the fast neutron spectrum. This effect combined with the relatively long heat transfer time constant for oxide fuel promotes reactor stability and tends to terminate a power excursion resulting from accidental insertion of a fairly appreciable positive reactivity step. Additional safety advantages associated with a large core size and an oxide-fueled reactor are:

(1) a small excess operating reactivity associated with a fairly long refueling cycle, and (2) diminution of the reactivity increment resulting from a possible fuel slump as well as from motion of the fuel and structural components (such as the EBR I fuel element oscillations).[1]

A positive sodium temperature coefficient of reactivity appears to be the principal safety disadvantage of a large fast oxide core since total loss of sodium may insert a large positive reactivity step. The positive sodium coefficient does not cause reactor instability if its magnitude is appreciably less ($\sim \frac{1}{2}$) than the negative Doppler coefficient. This condition can be satisfied with an appropriate choice of core dimensions and compositions. An essential safety design criterion is that the prompt negative Doppler reactivity effect be sufficiently large to terminate a power excursion resulting from total coolant loss before bulk fuel meltdown occurs.

In order to define the domain of reactor dimensions and compositions that yield acceptable reactor safety parameters, calculations were made of physics safety parameters for blanketed and reflected cores of varying size and composition. Physics safety parameters included the following:

(1) Doppler coefficient; its variation with temperature; total negative reactivity available from the Doppler effect for a power excursion starting from fuel at operating temperature for rated power, and also from room temperature for a startup accident; separate contributions to the Doppler coefficient by U-238, Pu-239, and Pu-240; dependence of the Doppler coefficient on neutron spectrum; effects of spatial temperature and power distributions.

(2) Sodium temperature coefficient; reactivity insertion due to total loss of coolant.

(3) Reactivity coefficients due to thermal expansion of fuel and steel clad.

(4) Excess operating reactivity that must be held down by control rods as a function of the fuel specific power and the refueling cycle.

(5) Reactivity insertion for a fuel slump resulting in 100% densification of the oxide fuel.

Neutron lifetime was calculated for a fast oxide reactor both with and without a beryllium reflector placed between the reactor and the radial blanket. Insertion of the beryllium tends to increase the neutron lifetime, as indicated by the Argonne National Laboratory studies on coupled fast-thermal reactors.[17] This, in turn, lessens the hazards associated with an accidental attainment of a prompt critical condition. Results of these calculations are given in Appendix I.

II Calculational Techniques

An 18-energy group cross section set was used for analysis of the reactivity coefficients. Multigroup cross sections for U-238, Pu-239 and

Pu-240 were calculated as a function of fuel temperature and of isotopic concentrations. The resolved resonance region for U-238 from 5 to 1000 ev was split into 4 groups. The region from 1000 to 9000 ev, containing unresolved but separated resonances were divided into two groups. The fast region, above 9 Kev with highly overlapping resonances was divided into 10-energy groups utilizing the Argonne National Laboratory fast reactor cross section set.(2)

Effective resonance integrals were calculated for each energy group, using Rosen's data for U-238 resonance parameters below 1000 ev.(3) A constant radiative capture width Γ_γ = .0246 ev, a Porter-Thomas distribution(4) of reduced neutron widths Γ_n^o with $< \Gamma_n^o >$ = .00176 ev, and an average resonance spacing of 18.5 ev from 1000 to 9000 ev were assumed. For Pu-240 resolved resonance parameters were available only up to 120 ev(5), and the statistical methods for unresolved resonances were used from 120 to 9000 ev with Γ_γ=.032 ev, $< \Gamma_n^o >$ = .0027 ev, and an 11.0 ev mean spacing between resonances. The reactor was assumed to be homogeneous for these calculations, which is a very good approximation for an oxide-fueled fast reactor. The RES Code, which was developed by Nordheim and Adler(6) and utilizes the methods of Dresner(7) for evaluation of Doppler broadened resonance integrals in homogeneous cores, was used for these calculations.

For Pu-239, resolved resonance parameters were available only up to 60 ev, which is not the region of interest. For the unresolved resonances up to 9000 ev, the following assumptions were made.

(1) The resonance fission width Γ_f follows a three-degree-of-freedom Porter-Thomas statistical distribution.(8)

(2) The ratio $< \Gamma_f > / \Gamma_\gamma$ as a function of energy is the same as the energy dependence of the Pu-239 alpha value (See Appendix II).

(3) Γ_γ is constant at .039 ev, Γ_n^o follows the usual one-degree-of-freedom Porter-Thomas distribution(4) with $< \Gamma_n^o >$ = .000661 ev, and the average resonance spacing is 2.5 ev.

(4) Γ_f / Γ_γ is constant over each resonance (Breit-Wigner single-level approximation).

(5) A statistical weight factor of 1/2 for each Pu-239 spin state is adequate (instead of the actual 1/4 and 3/4 values which increase the computational requirements).

With these assumptions, the Pu-239 resonance self-shielding could be treated the same as for U-238, simply by using the sum $\Gamma_\gamma + \Gamma_f$ in place of just Γ_γ and allowing for the statistical fluctuation of Γ_f. Appendix II describes in greater detail the calculational procedures used for evaluation of the Pu-239 resonance integrals.

In the 10 high-energy groups, which do not contribute much to the Doppler coefficient, the method of Feschbach, Geortzel and Yamauchi(9) was used to compute the change in the U-238 capture cross section with fuel temperature.

A code, HEDO, was developed for the calculation[10]. In this high energy region each Pu-239 atom was assumed to contribute a positive Doppler reactivity effect which has $1\frac{1}{2}$ the magnitude of that of each U-238 atom. This is based on Bethe's analysis of the U-235 Doppler effect for partially enriched uranium fast reactors[8] and takes into account the higher ($\nu\sigma_f - \sigma_a$) for Pu-239. The Doppler effect for Pu-240 in the 10 high-energy groups was neglected since it has almost zero reactivity worth over most of this energy region.

Spatial averaging of the Doppler coefficient to yield an effective prompt negative power coefficient was carried out, taking into account both the gross fuel temperature distribution over the core and the radial temperature distribution over a single fuel rod. Equations for these calculations and assumptions upon which they are based are given in Appendix IV.

The safety parameters reported are all results of 18-group, one-dimensional diffusion calculations. Doppler effects were obtained by performing calculations at several different fuel temperatures. Breakdown of the Doppler coefficient into isotopic components was accomplished by changing the temperature of one isotope at a time. Considering reactors with 10 percent and 100 percent loss of sodium yielded the sodium loss effects, while the clad and fuel coefficients resulted from calculations with 10 percent axial expansion of the clad and fuel separately. In these calculations it was assumed that the reactivity change from varying one component is independent of the others. Eighteen-group cross sections for fuel isotopes at various temperatures and for fission product pairs are given in Appendix III.

III CASES CALCULATED

Table IA lists the fast oxide reactor cases covered in the calculations classified according to core size, shape, composition and blanketing. Core fuel isotopic compositions yielding criticality are given for each case for an average fuel burnup of 50,000 MWD/t. (This is the average burnup for a core in which the depleted fuel is withdrawn at 100,000 MWD/t irradiation exposure.) The isotopic plutonium composition is assumed to be 2/3 Pu-239 and 1/3 Pu-240.* Slab geometry was assumed for all of the cases except those involved in the evaluation of the fuel slump effect (see Table VI) where it is important to distinguish between the axial and radial neutron leakage components and several radial cases used to check radial leakage estimations. For physics safety parameters other than the slump effect, the slab results may be applied to cylindrical cores having identical neutron leakage and composition. One-dimensional multigroup calculations were made to determine radial leakage characteristics for reactors corresponding to several of the slab cases but having L/D ratios of $\frac{1}{4}$, $\frac{1}{2}$ and 1. Table IA

*Lack of resonance data for the higher plutonium isotopes necessitated specifying all of the fissile isotopes (Pu-239 + Pu-241) as Pu-239 and all of the even isotopes (Pu-240 and Pu-242) as Pu-240. In earlier fuel cycle calculations the input plutonium isotopic composition was taken as that of the output from a thermal reactor.[11] The ratio of Pu(239 + 241) to Pu(240 + 242) after 50,000 MWD/t burnup was found to be very nearly two over a wide range of core sizes and compositions.

TABLE IA

CASES CONSIDERED IN FOB SAFETY EVALUATION
(Fuel is 90% Theoretical Density)

Case No.	Sodium Volume Fraction[a]	$\frac{V_{fuel}}{V_{steel}}$	Core Length Ft.	Core Diameter Ft.	Blanket Thickness Inches	Pu-239 Atom Fraction(%)[b]
1	.10	2	2	∞	15	10.0
2	.10	2	3	∞	15	8.96
3	.30	2	1.5	∞	15	12.2
4	.30	2	2	∞	15	10.9
5	.30	2	3	∞	15	9.7
6	.30	3	1.5	∞	15	11.4
7	.30	3	2	∞	15	10.1
8	.50	2	2	∞	15	12.8
9	.50	2	3	∞	15	11.1
10	.50	2	5	∞	15	9.75
11	.50	3	1.5	∞	15	13.6
12	.50	3	2.0	∞	15	12.0
13	.70	2	3	∞	15	14.3
14	.70	2	5	∞	15	11.8
15[c]	.10	2	2.41	9.64	15	10.0
16[c]	.30	2	2.46	9.84	15	10.9
17[c]	.30	2	3.5	14.0	15	9.7
18[c]	.50	2	2.48	9.92	15	12.8
19[c]	.50	2	3.21	6.42	15	12.8
20[c]	.50	2	7.1	14.2	15	9.75
21[c]	.50	2	10.5	10.5	15	9.75
22	.50	2	2	∞	Na-SS Reflector[d]	12.8
23	.50	2	3	∞	Na-SS Reflector[d]	10.8
24	.50	2	5	∞	Na-SS Reflector[d]	9.6

a Fuel and steel compose the remainder of the core. Insertion of small volumes of void for control channels will not significantly change the results.

b Based upon the quantity of U-238, Pu-239, Pu-240 and fission product pairs. Atom fraction of fission product pairs is 5.8% corresponding to 50,000 MWD/t burnup, and atom fraction of Pu-240 is $\frac{1}{2}$ that of Pu-239.

CONT'D FROM TABLE IA

c Cases 15 through 21 are cylindrical cases equivalent to cases 1, 4, 5, 8, 8, 10 and 10, respectively.

d Same composition as core, but with stainless steel inserted for fuel.

lists the L values (core lengths) for both the slab and equivalent cylindrical cases; Figure 1 shows the equivalent dimensions of cylindrical reactors corresponding to the slab cases.

Isotopic compositions for each case in each of the 5 geometric regions of the 15-inch thick axial and radial blankets are listed in Table IB. These correspond to the estimated isotopic buildup after 50,000 MWD/t core burnup, starting with depleted uranium in the blanket. Sodium and steel volume fractions in the axial blankets were taken equal to those of the core. Volume fractions in the radial blankets were varied from core values to values giving low sodium and steel content. For cores with small L/D the axial blanket will be more important than the radial blanket, resulting in fuel economics not greatly different from those of the slab cases. For greater L/D, the slab cases will give slightly pessimistic fuel economics since larger fuel volume fractions in the radial blankets will result in higher total breeding ratios.

IV RESULTS

A. Doppler Coefficient

Table II lists the contributions to the Doppler coefficient from each energy group for case 23. These results show the importance of the intermediate energy resonance region to the Doppler coefficient of a large fast oxide reactor. Although 80% of the power spectrum occurs above 9 kev, this fast energy region contributes only 10% of the Doppler coefficient. About 75% of the Doppler reactivity change is contributed by the energy region between 300 and 4000 ev. The Doppler coefficient for the large fast oxide reactor is 5 to 10 times greater than that for a small relatively highly enriched metal-fueled fast reactor such as FERMI I,[12] which does not have the appreciable low energy tail in its power spectrum. Recent calculations carried out independently at APDA also yielded the appreciable Doppler coefficient (-1×10^{-5} $\Delta k/k\text{-}^{\circ}C$) for a large fast oxide reactor.[13]

Table II also shows the contribution of each of the fuel isotopes to the Doppler coefficient. It is somewhat disturbing that the Pu-239 contributes a positive Doppler effect about 40% the magnitude of the negative contribution by the U-238, in spite of the 1:7 isotopic ratio. This indicates that smaller fast reactors requiring higher Pu-239 content may not have a significant negative Doppler coefficient and, in fact, very small reactors would have positive coefficients.

Figure 2 shows the decrease in reactivity with increasing fuel temperature due to the Doppler effect. The four curves cover core sizes of 2 and 3 feet, with sodium volume fractions of 30 and 50 percent. (Cases 4, 5, 8, and 9 in Table L)

The Doppler coefficient at a given fuel temperature is the slope of the curves plotted in Figure 2. For example, the coefficient is -2.8×10^{-5}, -0.84×10^{-5} and -0.37×10^{-5} $\Delta k/k\text{-}^{\circ}C$ respectively for 20, 900, and 2750°C fuel temperature for the 3 ft slab case with 50 percent sodium. As expected, this is approximately a 1/T variation, where T is the absolute temperature.

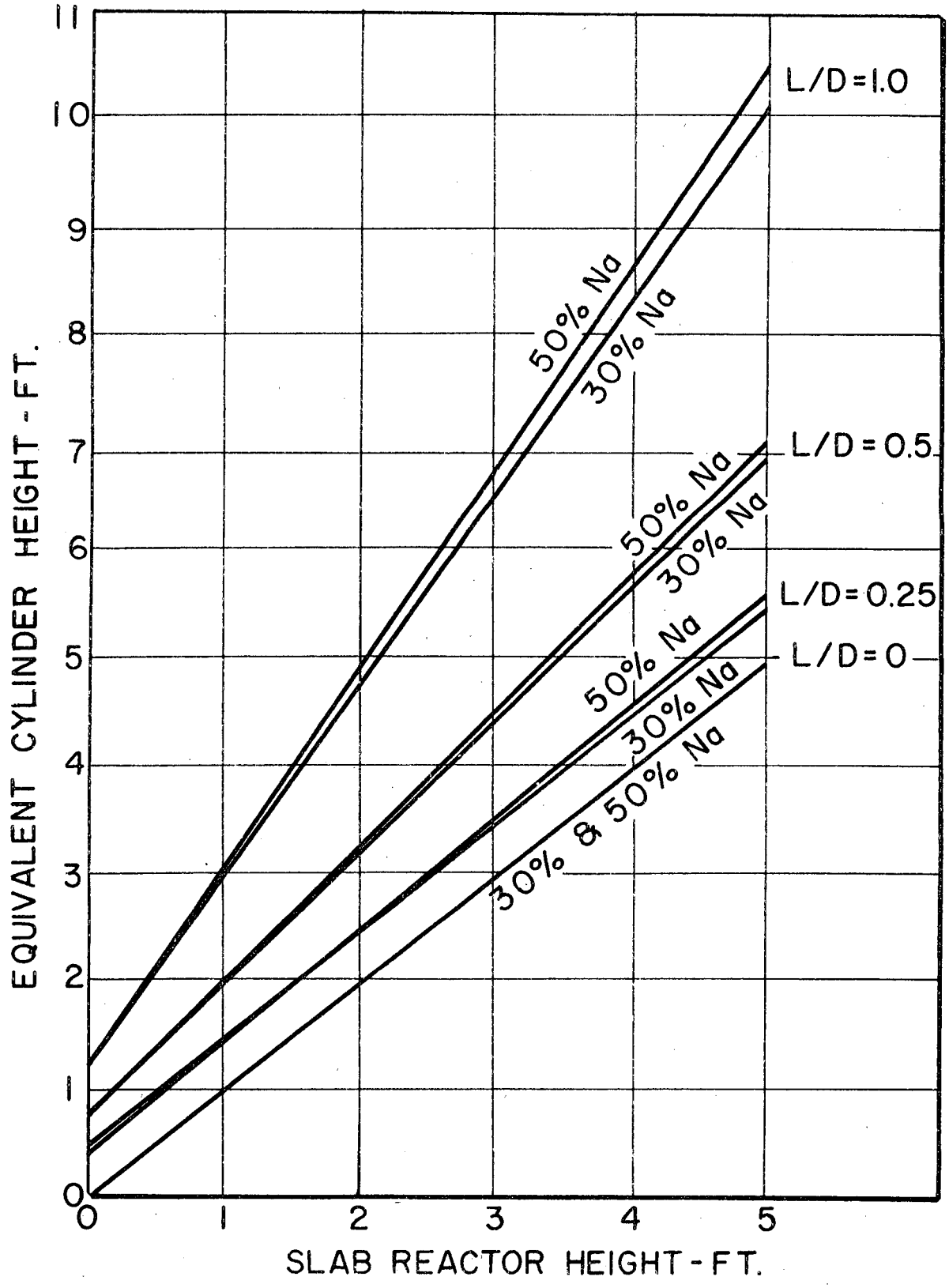

Figure 1 - Equivalent Cylinder Dimensions for Blanketed Slab Reactors Containing 30 and 50% Sodium.

TABLE IB

BLANKET COMPOSITIONS

Case No.	Sodium Volume Fraction	$\frac{V_{fuel}}{V_{steel}}$	Equilibrium Pu-239 & Fission Product Pair Atom Fractions[a] (Percent) Pu-239 REGION 1	2	3	4	5	Fission Product Pairs REGION 1	2	3	4	5
1	.10	2	2.77	2.25	1.71	1.24	.87	1.45	.81	.45	.24	.14
2	.10	2	1.43	1.16	.89	.64	.45	.48	.27	.15	.08	.04
3	.30	2	3.99	3.23	2.46	1.79	1.25	2.83	1.57	.87	.48	.26
4	.30	2	3.42	2.77	2.11	1.53	1.07	1.85	1.02	.56	.29	.17
5	.30	2	2.40	1.95	1.49	1.08	.75	.85	.48	.26	.14	.08
6	.30	3	3.98	3.23	2.46	1.79	1.25	3.04	1.70	.93	.52	.28
7	.30	3	3.43	2.78	2.12	1.54	1.08	2.02	1.12	.61	.35	.19
8	.50	2	4.09	3.32	2.53	1.84	1.28	2.23	1.24	.69	.37	.20
9	.50	2	3.19	2.59	1.97	1.43	1.00	1.17	.65	.35	.20	.10
10	.50	2	1.70	1.38	1.05	.76	.53	.38	.21	.11	.06	.03
11	.50	3	4.57	3.71	2.83	2.05	1.44	3.31	1.84	1.02	.52	.30
12	.50	3	4.09	3.32	2.53	1.83	1.28	2.32	1.29	.72	.39	.21
13	.70	2	4.56	3.70	2.82	2.05	1.43	1.48	.82	.45	.25	.13
14	.70	2	2.64	2.14	1.63	1.19	.83	.53	.30	.17	.09	.05
15[b]	.15	2	1.16	.94	.72	.52	.36	.13	.07	.04	.02	.01
16[b]	.15	2	1.11	.90	.69	.50	.35	.13	.07	.04	.02	.01
17[b]	.15	2	.92	.75	.57	.41	.29	.07	.04	.02	.01	.01
18[b]	.50	2	2.19	1.77	1.35	.98	.69	.24	.14	.08	.04	.02
19[b]	.50	2	2.50	2.03	1.55	1.12	.79	.56	.32	.17	.09	.05
20[b]	.50	2	.61	.49	.38	.27	.19	.08	.04	.02	.01	.01
21[b]	.50	2	.87	.71	.54	.39	.27	.17	.10	.05	.03	.02

a Both the top and bottom axial and radial blankets are divided into five regions, each 3 inches thick, initially loaded with depleted uranium (0.4% U-235). Equilibrium fuel refers to blanket fuel which has been present in the reactor for 50,000 MWD/t burnup in the core.

b Denotes radial blanket. All other compositions listed are for the top and bottom axial blankets.

TABLE II

ENERGY SPECTRUM OF DOPPLER COEFFICIENT[a]

Energy Group No.	Δu	E_L ev	$(dk/dT)_{Dop}$ - $(\Delta k/k^{\circ}C \times 10^6)$ U-238	Pu-239	Pu-240	Total	Accumulative Total
1	1.5	2.25×10^6	0	0	0	0	0
2	0.5	1.35×10^6	0	0	0	0	0
3	0.5	8.25×10^5	0	0	0	0	0
4	0.5	5.0×10^5	0	0	0	0	0
5	0.5	3.0×10^5	0	0	0	0	0
6	0.5	1.8×10^5	-.014	+.003	0	-.011	-.011
7	0.5	1.1×10^5	-.031	+.006	0	-.025	-.036
8	0.5	6.7×10^4	-.081	+.017	0	-.064	-.100
9	1.0	2.5×10^4	-.261	+.054	0	-.207	-.307
10	1.0	9100	-.559	+.116	0	-.443	-.750
11	0.8	4000	-.866	+.065	-.019	-.820	-1.570
12	1.4	1000	-3.257	+.316	-.138	-3.079	-4.649
13	1.2	300	-3.900	+1.342	-.562	-3.120	-7.769
14	1.1	100	-1.516	+1.664	-.415	-.267	-8.036
15	1.2	30	-.332	+.357	-.247	-.222	-8.258
16	1.8	5	-.083	+.260	-.019	+.158	-8.100
17	2.5	0.4	0	0	0	0	-8.100
18	---	0	0	0	0	0	-8.100
Total	---	---	-10.9	+4.2	-1.4	-8.1	-8.1

a Data presented is for Case No. 23. The spectral distribution of the Doppler effect above is based upon the simplifying assumption that the neutron importance is constant for all energy groups. To this extent the spectral breakdown is approximate. The total Doppler coefficients (bottom row of data) were obtained directly from multigroup calculations and do not involve this assumption, and have not been corrected for temperature distributions.

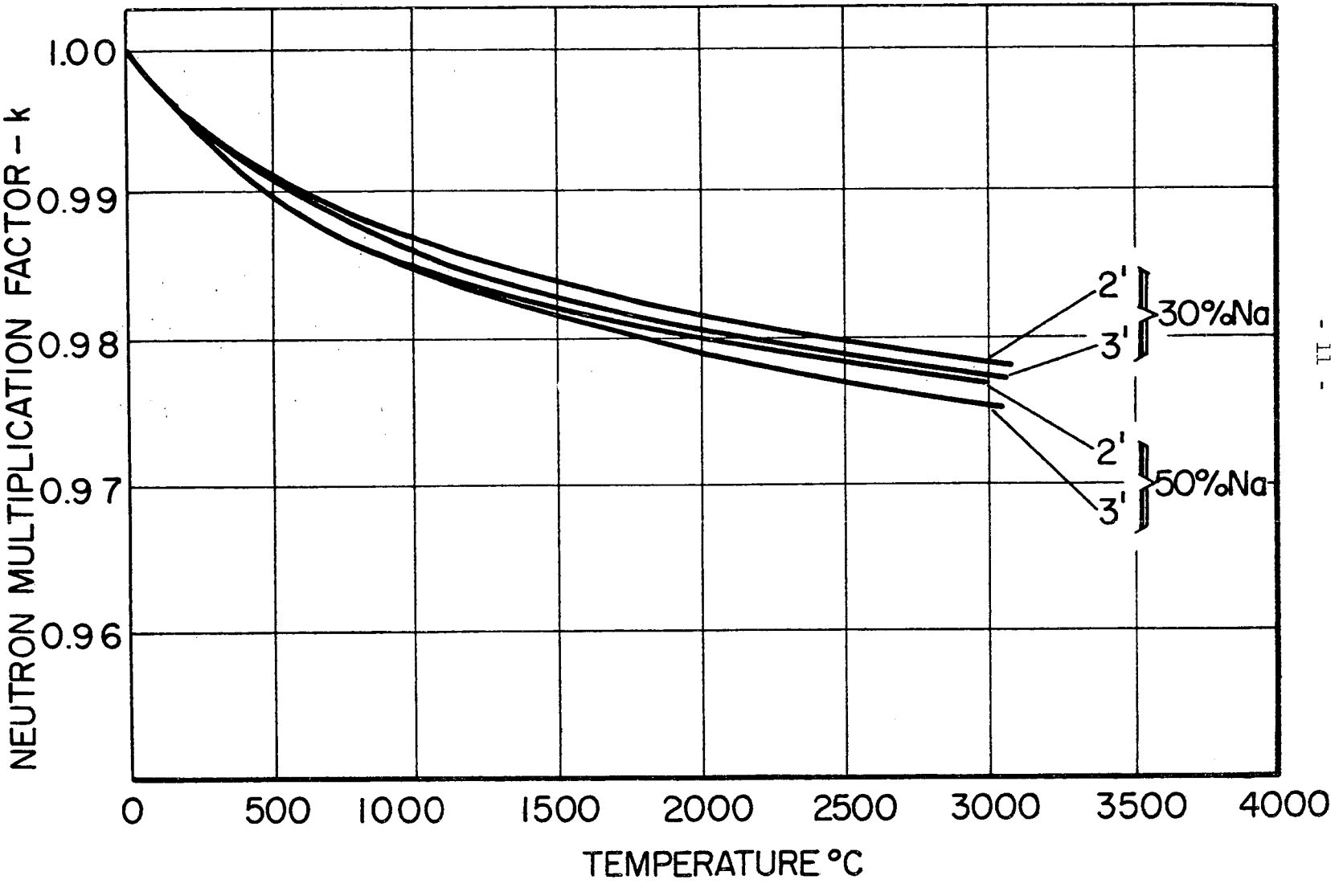

Figure 2 - Neutron Multiplication Factor Versus Average Fuel Temperature (Doppler Effect)

Note from Figure 2 that most of the prompt shutdown reactivity available from the Doppler effect occurs between room temperature and the average fuel operating temperatures ($\sim$ 900°C). The available negative reactivity from operating temperature to fuel melting temperature ($\sim$ 2750°C) is only about 40% of the total.

Table III lists Doppler coefficients for the reactor cases covered in Table IA. Also listed are the values of the total negative reactivity available, $(\Delta k)_{Dop}$, as a result of the Doppler effect. The values $(\Delta k)_{Dop}$ represent the negative reactivity provided by the Doppler effect as the result of a rapid power transient in which the fuel temperature in the region of peak power reaches its melting point. Using pelletized fuel as a model for this criterion, $(\Delta k)_{Dop}$ gives the negative reactivity feedback provided by the Doppler effect when the hottest fuel pellet uniformly reaches its melting temperature (allowing also for the heat of fusion before the pellet reaches this temperature). Values of $(\Delta k)_{Dop}$ are listed in Table III for (a) the fuel initially at room temperature, representing a power excursion at startup, and (b) the fuel temperature distribution initially at operating conditions (900°C average) representing a power excursion from the normal full power operating conditions. Conditions (a) and (b) are more fully explained in Appendix IV. In either case, the last several hundred degrees of fuel temperature rise do not contribute significantly to the Doppler reactivity change.

There are no experimental data available to verify the large calculated Doppler coefficient. Measurements by Frost of the U-238 Doppler effect in a U-235 fueled critical assembly operating in an intermediate spectrum yielded a large negative coefficient.[14] This result is in qualitative agreement with the present Doppler calculations although the critical experimental conditions were too different from a fast oxide reactor to provide quantitative substantiation of the calculated results.

B. Sodium Reactivity Coefficient

Table IV shows the reactivity change resulting from 10% and 100% removal of the sodium from the reactor cases covered. For these calculations the sodium is assumed to be uniformly removed from the core and the blanket or reflector. The sodium temperature coefficient of reactivity based on the 10% removal calculations is also listed in Table IV. Major concern is in the reactivity insertions which could result from a total loss of coolant accident, as this appears to be the principal safety limitation on the core size.

For the large fast oxide reactor cases that appear desirable for most other safety and economic considerations, the sodium temperature coefficient is positive. For all cases except the largest of the core sizes considered, the magnitude of the sodium coefficient is significantly less than that of the Doppler coefficient. This should insure reactor stability for these cases.

TABLE III

DOPPLER COEFFICIENTS AND TOTAL AVAILABLE REACTIVITY

DECREASE DUE TO DOPPLER EFFECT

Case No.	$(dk/dT)_{Dop}$ - $\Delta k/k$-°C x 10^6 At Average Fuel Temp. 900°C	$(dk/dT)_{Dop}$ - $\Delta k/k$-°C x 10^6 Weighted[a] Average	Available Reactivity Change Due to Doppler Effect[b] $(\Delta k)_{Dop}$ - Dollars From Room Temp. 20°C	Available Reactivity Change Due to Doppler Effect[b] $(\Delta k)_{Dop}$ - Dollars From Operating Temp. 900°C Avg.
1	-7.0	-8.6	-4.4	-1.5
2	-7.1	-8.7	-4.5	-1.5
3	-6.9	-8.5	-4.6	-1.5
4	-7.6	-9.3	-4.8	-1.7
5	-7.9	-9.7	-5.0	-1.7
6[c]	-6.9	-8.5	-4.4	-1.5
7[c]	-7.3	-9.0	-4.4	-1.5
8	-7.6	-9.3	-5.4	-1.8
9	-8.4	-10.3	-5.6	-2.0
10	-8.9	-10.9	-6.0	-2.2
11[c]	-6.5	-8.0	-4.5	-1.6
12[c]	-7.6	-9.3	-5.1	-1.8
13	-8.5	-10.5	-6.1	-2.4
14	-11.3	-13.9	-7.4	-2.8
22[d]	-6.7	-8.2	-4.9	-1.7
23[d]	-8.1	-10.0	-5.3	-2.0
14[d]	-9.2	-11.3	-6.0	-2.3

a The weighted average Doppler coefficient is spatially averaged as a prompt power coefficient using the relationships derived in Appendix IV.

b See Appendix IV for the derivation of $(\Delta k)_{Dop}$.

c Cases for $V_{fuel}/V_{steel} = 3.0$.

d Blanket is replaced by a reflector with stainless steel inserted for fuel.

TABLE IV

REACTIVITY TEMPERATURE COEFFICIENTS AND STEP REACTIVITY CHANGES DUE TO LOSS OF SODIUM

Case No.	Sodium Content %	Slab Height Ft.	Change in Reactivity Due to Sodium Loss 10% $	Change in Reactivity Due to Sodium Loss 100% $	Reactivity Coefficients $\Delta k/k^{\circ}C \times 10^6$ $(dk/dT)_{Sod}$ [a]	$(dk/dT)_{Clad}$ [b]	$(dk/dT)_{Fuel}$ [b]
1	10	2	+.10	+1.1	+1.1	+.95	-1.13
2	10	3	+.15	+1.5	+1.7	+1.21	-1.24
3	30	1.5	+.14	+1.4	+1.5	+.35[c]	-1.49[c]
4	30	2	+.26	+2.7	+2.8[c]	+.66	-1.66[c]
5	30	3	+.41	+4.4	+4.5	+.99	-1.86
6[d]	30	1.5	+.16	+1.7	+1.8	~+.35[d]	~-1.49[d]
7[d]	30	2	+.27	+2.9	+3.1	~+.66[d]	~-1.66[d]
8	50	2	+.10	+0.1	+1.0	+.38	-1.27
9	50	3	+.49	+5.0	+5.1	+.68	-1.57
10	50	5	+1.05	+11.0	+11.0	+1.08	-1.98
11[d]	50	1.5	-.09	-2.2	-0.9	~+.08[d]	~-1.08[d]
12[d]	50	2	+.17	+1.0	+1.8	~+.38[d]	~-1.27[d]
13	70	3	-.27	-11.4	-2.5	+.32	-.84[c]
14	70	5	+.87	+6.6	+8.4	+.38	-1.42[c]
22[e]	50	2	+.36	+3.4	+3.5	+.58[c]	-1.86[c]
23[e]	50	3	+.61[c]	+6.6[c]	+6.3[c]	+.88[c]	-2.04[c]
24[e]	50	5	+.98	+11.2	+10.3	+.94	-2.59

a The values of $(dk/dT)_{Sod}$ do not include variation in sodium volume due to clad and other structural expansion.

b (dk/dT) due to axial expansion only. Linear thermal expansion coefficients are $1.8 \times 10^{-5}/^{\circ}C$ for clad and $1.3 \times 10^{-5}/^{\circ}C$ for fuel.

c Extrapolated or interpolated from results of calculated cases.

d Cases for $V_{fuel}/V_{steel} = 3.0$ $\left[(dk/dT)_{clad}\right.$ and $\left.(dk/dT)_{fuel}\right]$ were not calculated so they are assumed to have same values as equivalent cases with $V_{fuel}/V_{steel} = 2.0$.

e Blanket is replaced by a reflector with stainless steel inserted for fuel.

Figure 3 shows the sodium temperature coefficient as a function of sodium volume fraction for a range of core sizes (all with 15-inch thick blankets). Characteristically the coefficient attains a peak value at intermediate sodium volume fractions with the peak falling at higher sodium volume fractions for the larger cores. This peaking can be explained by considering the competitive processes that yield the overall sodium temperature coefficient. As described by Zweifel and Nims[15] the positive component of the temperature coefficient arises from spectral hardening due to reduced sodium elastic and inelastic scattering. The negative component arises from increased neutron leakage.

At intermediate sodium volume fractions the positive spectral component dominates and the resulting coefficient is positive. As the sodium content is increased, the positive spectral effect tends to reach saturation level while the leakage effect becomes increasing more negative. This results in a coefficient which likewise becomes increasingly more negative with increasing sodium content, as observed on the right side of the peak values in the curves of Figure 3. Since leakage is an inverse function of the core size, the negative leakage component dominates at low sodium volume fractions for small reactors, while it takes high sodium volume fractions for leakage to dominate the sodium coefficient of a large core. Figure 3 shows this effect with the large cores having both more positive coefficients and peak values at higher sodium volume fractions. Reactors with greater fuel-to-steel ratios will have less leakage for the same size and sodium content, resulting in more positive sodium coefficients.

On the left side of the peak the sodium content is so small that the sodium becomes ineffectual. Thus the sodium temperature coefficient approaches zero as the sodium volume fraction approaches zero even though the positive component still dominates.

Figure 4 shows the reactivity gain as a function of fractional sodium loss. For the large core sizes where neutron leakage is not highly sensitive to the sodium removal, the reactivity increases slightly more than linearly with sodium removal. For a 2-foot core with 50% sodium (high neutron leakage) the sodium removal reactivity coefficient which is initially positive, becomes negative at about 50% sodium removal. In this case fractional loss of sodium may insert more reactivity than 100% loss of sodium.

C. Fuel and Steel Clad Axial Expansion Reactivity Coefficients

Table IV shows the reactivity temperature coefficient due to steel clad axial expansion. The steel reactivity worth is more negative than that of the sodium for nearly all cases considered. However, the positive temperature coefficient due to steel axial expansion is generally less than that of the sodium since the steel has a much smaller thermal expansion coefficient.

The negative temperature coefficient due to fuel axial expansion is also listed in Table IV. For the large oxide-fueled reactors, the fuel axial expansion coefficient is small compared with the Doppler coefficient. Also, it is not certain as to how much the axial expansion effect can be depended upon with oxide fuel which is subject to cracking and contains

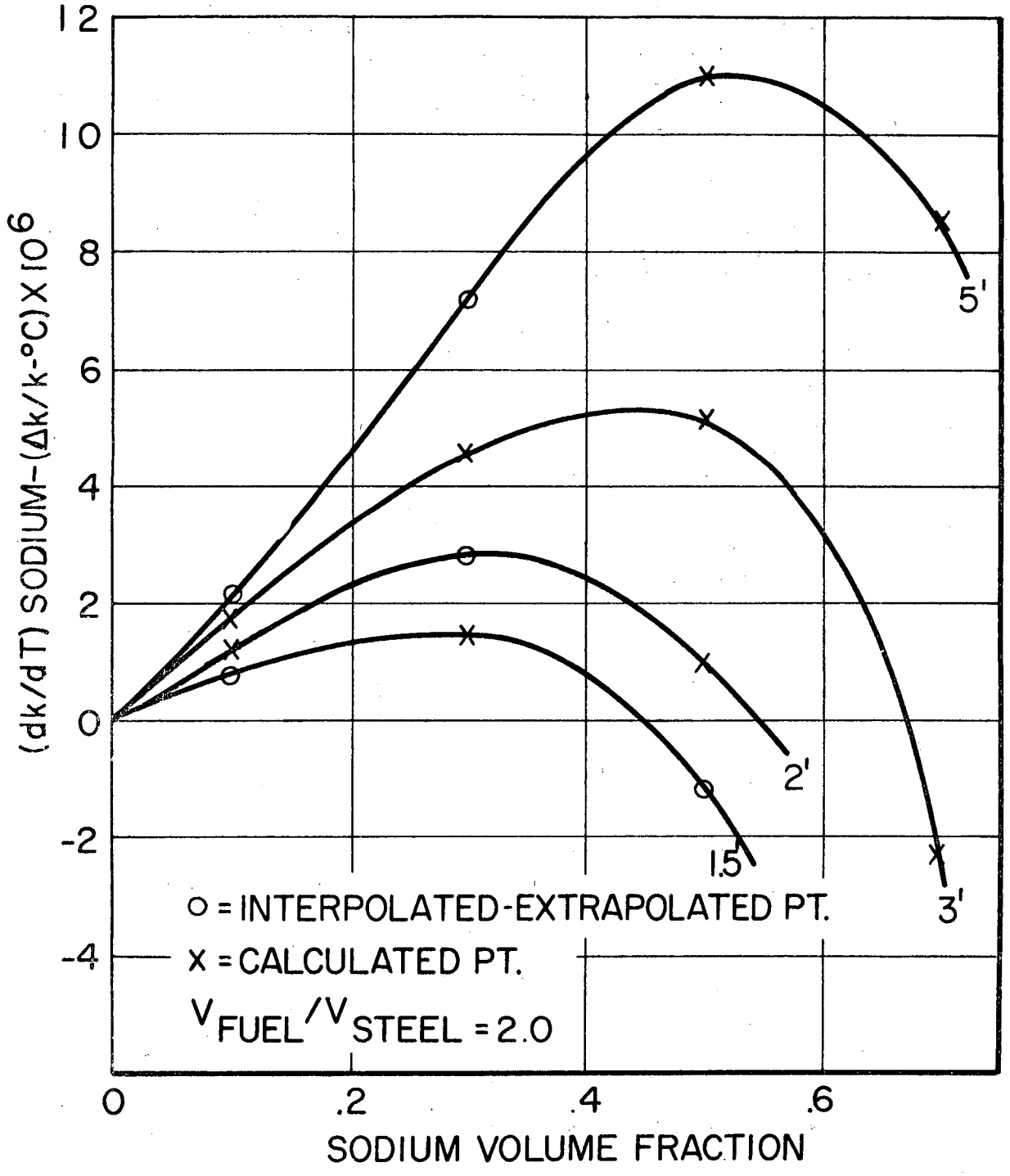

Figure 3 - Sodium Coefficient Versus Volume Fraction of Sodium in Blanketed Core.

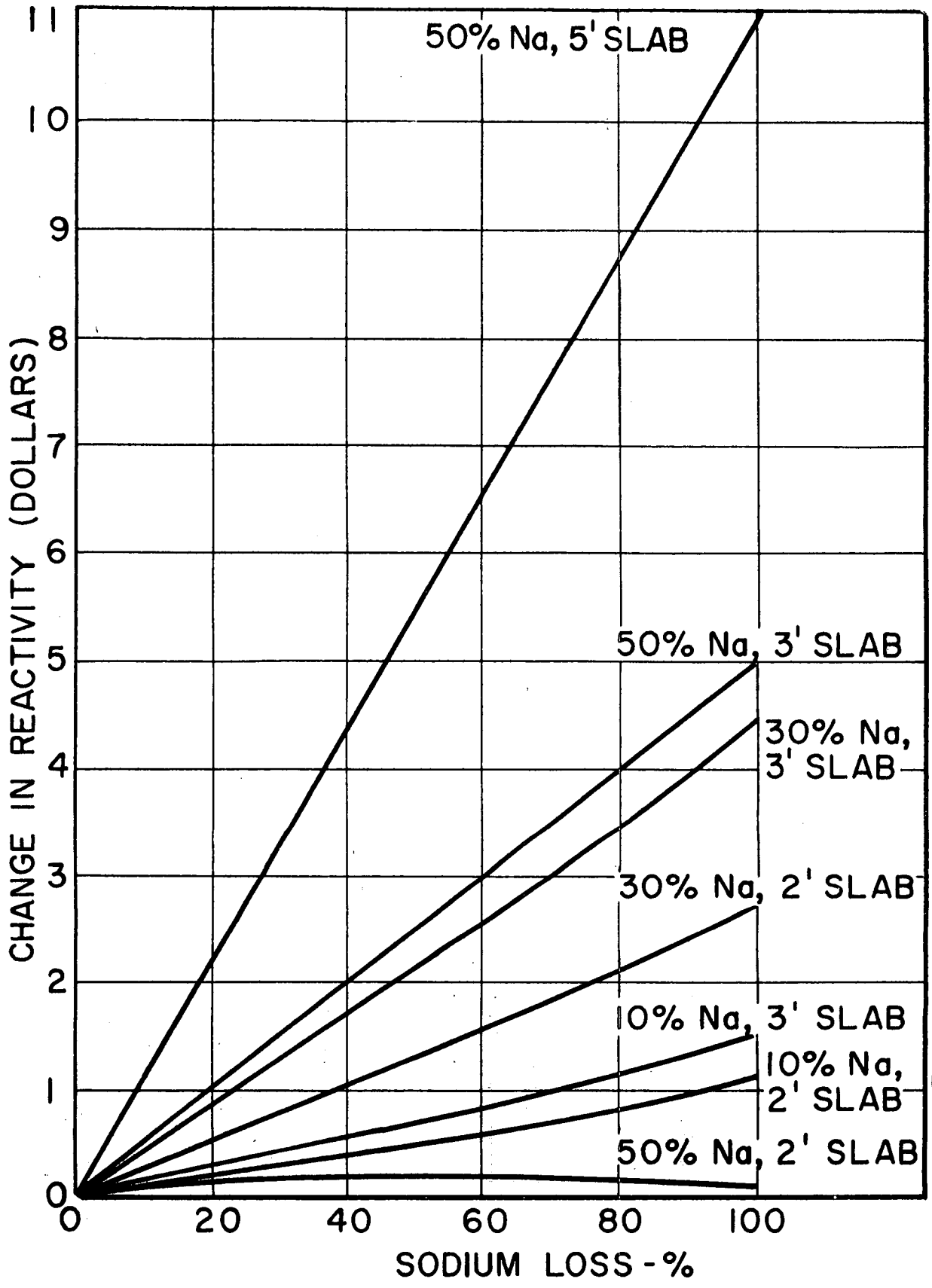

Figure 4 - Change in Reactivity Versus Percent of Sodium Loss from Core and Blanket.

voids into which individual particles can expand.

Radial expansion of the fuel and its supporting structure are not taken into account in the calculated temperature coefficients listed in Table IV since they are contingent upon a specific design. For example, radial expansion of the clad would tend to reduce the sodium content thereby contributing a positive reactivity effect. On the other hand, overall thermal expansion of the core and its subassembly structural components would tend to reduce reactivity. The relative importance of these two effects depends upon the reactor design.

D. Excess Operating Reactivity Requirements and Breeding Ratios

A safety characteristic favoring a core with low neutron leakage (large size and low sodium content) is the relatively low excess operating reactivity which must be held down by control rods. For a given fuel specific power, plant load factor, and refueling interval, this excess operating reactivity is dependent upon the core breeding ratio. Table V lists values of the excess operating reactivity requirement, $(\Delta k)_{Rod}$ for a fuel specific power of 1000 kw/kg Pu-239, a 3-month refueling interval, and a 0.8 load factor. The core and total breeding ratios are also listed. Excess operating reactivities for other combinations of fuel specific power, refueling interval, and load factor may be deduced from the data of Table V by assuming a linear dependence of the operating reactivity upon these factors.

E. Fuel Slump Reactivity Insertion

The possibility of redistribution and densification of the oxide fuel in a meltdown has been classified as a potential safety hazard, since the initial oxide fuel density is less than its theoretical value. Table VI shows the reactivity insertion resulting from a densification of the oxide fuel to its theoretical value, resulting in a shorter core length. Core diameter and content of steel and sodium were assumed invariant under the fuel slump. Core composition and size, oxide fuel density, and neutron leakage before slump occurs are also listed in Table VI.

For fuel at 65% theoretical density, the fuel slump reactivity insertion is sufficiently great that a possible slump might be impossible to control. This applies even for a partial slump which does not include all of the fuel or does not go to 100% theoretical density. Increasing the normal fuel density from 65% to 90% theoretical reduces the fuel slump reactivity insertion by a factor of four. Going to a larger core size with lower neutron leakage further reduces the slump reactivity effect, and an appreciable diminution of the fuel slump effect is achieved by utilizing a core with low L/D (the extreme case of a slab is included in Table VI). Since fuel slumping to near 100% theoretical density is not probable, this effect does not appear to be a major problem over the range of reactor sizes which show promise. Fuel motion in the form of fuel rod bowing is another potential safety hazard. This likewise, is reduced in large reactors with a low length to diameter ratio, and proper fuel support design can reduce it to within safe limits.

TABLE V

EXCESS OPERATING REACTIVITY AND BREEDING RATIOS

Case No.	Sodium Content%	Slab Height Ft.	Excess Operating Reactivity,[a] $(\Delta k)_{Rod}$ - $	Core Conversion Ratio[b]	Total Breeding Ratio[c]
1	10	2	-0.06	0.97	1.30
2	10	3	-1.04	1.10	1.32
3	30	1.5	+1.44	0.78	1.20
4	30	2	+1.02	0.86	1.20
5	30	3	-0.24	1.02	1.25
6[d]	30	1.5	+0.78	0.83	1.26
7[d]	30	2	-0.09	0.96	1.30
8	50	2	+2.40	0.75	1.08
9	50	3	+1.35	0.89	1.11
10	50	5	+0.03	1.03	1.16
11[d]	50	1.5	+2.40	0.69	1.10
12[d]	50	2	+1.68	0.80	1.13
13	70	3	+3.78	0.68	0.88
14	70	5	+2.84	0.84	0.97
22[e]	50	2	+3.96	0.76	0.76
23[e]	50	3	+1.71	0.91	0.91
24[e]	50	5	+0.15	1.04	1.04

a Maximum for three month refueling interval at specific power of 1000 kw/kgm (fissionable fuel), and a load factor of 0.8. A positive value of $(\Delta k)_{Rod}$ means the reactivity decreases with burnup.

b Defined as: $\frac{\text{(Capture in fertile material in core)}}{\text{(Absorption in fissile material in core)}}$

c Defined as: $\frac{\text{(Captures in fertile material in core and blanket)}}{\text{(Absorptions in fissile material in core and blanket)}}$

d Cases for $V_{fuel}/V_{steel} = 3.0$.

e Blanket is replaced by a reflector with stainless steel inserted for fuel.

TABLE VI

FUEL SLUMP EFFECT[a]

Fuel Density % Theoretical	Pu-239 Atom Fraction[b]	Core Height Ft.	Core Diameter Ft.	% Core Leakage	Fuel Slump Effect - Δk
65	.169	5	5	31.6	0.13
90	.130	5	5	24.6	0.033
90	.119	6	6	19.9	0.028
90	.119	2.4	∞	19.9	0.015

a For reactors with a 50% sodium volume fraction, $V_{fuel}/V_{steel} = 2.0$, and a 15 inch blanket.

b The ratio of Pu-240 to Pu-239 atom fractions was taken to be 0.5. The concentration of fission product pairs was .058, corresponding to an average fuel burnup of 50,000 MWD/t for an equilibrium core.

V SIGNIFICANCE OF RESULTS FOR FAST OXIDE REACTOR SAFETY

For reactor stability, the prompt negative power coefficient (Doppler and fuel axial expansion) must override the sum of the positive coefficients due to sodium removal and steel axial expansion. Criteria for reactivity effects that yield inherent reactor safety over and above stability, are more difficult to define, but the following serve as a reasonable guide.

(a) In the event of an instantaneous total or partial loss of coolant, the available Doppler negative reactivity should be sufficiently great to terminate the power excursion before bulk fuel meltdown occurs.

(b) In the event that all control rods are instantaneously ejected, the available Doppler negative reactivity should be sufficiently great to terminate the power excursion before bulk fuel meltdown occurs.

In order to satisfy these safety criteria, it is essential that the following two conditions be satisfied:

(1) $$\frac{-(\Delta k)_{Dop}}{2} + 1 > (\Delta k)_{Sod}$$

(2) $$\frac{-(\Delta k)_{Dop}}{2} + 1 > (\Delta k)_{Rod}$$

A justification for choosing these conditions, based upon a very simplified kinetics calculation, is given in Appendix V.

Table VII lists for several cases:

(a) Total reactivity coefficients at operating conditions,

$$(dk/dT)_{total} = (dk/dT)_{Dop} + (dk/dT)_{Sod} + (dk/dT)_{Clad}$$

(b) Available negative reactivity from the Doppler effect for a fuel temperature rise from operating temperature at rated power to a temperature condition short of bulk fuel meltdown, $(\Delta k)_{Dop}$. (See Appendix IV)

(c) Reactivity increase for total loss of coolant, $(\Delta k)_{Sod}$; and

(d) Excess operating reactivity, $(\Delta k)_{Rod}$.

The (Δk) values are given in dollar reactivity units, and the delayed neutron fraction for each case is also listed.

In order to satisfy condition (1), the smaller core sizes are favored, and a high sodium content, which increases neutron leakage, appears also as an advantage. However, condition (2) for reasonable values of fuel specific power and refueling intervals favors low sodium content and a large core size. Simultaneously satisfying conditions (1) and (2),

TABLE VII

FOB SAFETY PARAMETERS

Case No.	Sodium Content %	Slab Height Ft.	[a] $(dk/dT)_{Total}$ $\Delta k/k^{o}C \times 10^{6}$	Total Change in Reactivity-$ $(\Delta k)_{Dop}$	$(\Delta k)_{Sod}$	[b] $(\Delta k)_{Rod}$	Delayed Neutron Fraction
1	10	2	-6.55	-1.5	+1.1	-0.06	0.0039
2	10	3	-5.79	-1.5	+1.5	-1.04	0.0040
3	30	1.5	-6.65	-1.5	+1.4	+1.44	0.0037
4	30	2	-5.84	-1.7	+2.7	+1.02	0.0038
5	30	3	-4.21	-1.7	+4.4	-0.24	0.0039
6[c]	30	1.5	-6.35	-1.5	+1.7	+0.78	0.0039
7[c]	30	2	-5.24	-1.5	+2.9	+0.09	0.0040
8	50	2	-7.92	-1.8	+0.1	+2.40	0.0036
9	50	3	-4.52	-2.0	+5.0	+1.35	0.0037
10	50	5	+1.18	-2.2	+11.0	+0.03	0.0037
11[c]	50	1.5	-8.82	-1.6	-2.2	+2.40	0.0036
12[c]	50	2	-7.12	-1.8	+1.0	+1.68	0.0037
13	70	3	-12.68	-2.4	-11.4	+3.78	0.0033
14	70	5	-5.12	-2.8	+6.6	+2.84	0.0034
22[d]	50	2	-4.12	-1.7	+3.4	+3.96	0.0035
23[d]	50	3	-2.82	-2.0	+6.6	+1.71	0.0036
24[d]	50	5	+0.06	-2.3	+11.2	+0.15	0.0037

a Does not include negative contribution due to fuel axial expansion because of the uncertainty of this being available.

b Maximum three month refueling interval at specific power of 1000 kw/kg (fissionable fuel), and a load factor of 0.8. A positive value of $(\Delta k)_{Rod}$ means the reactivity decreases with burnup.

c Cases for $V_{fuel}/V_{steel} = 3.0$.

d Blanket is replaced by reflector for tnese cases.

along with obtaining an overall negative temperature coefficient, is most easily achieved by minimizing the sodium volume fraction and selecting a core size sufficiently small to satisfactorily limit $(\Delta k)_{Sod}$. Taking Case 1 in Table VII as an example, with 10% sodium volume fraction and a 2-ft core length, conditions (1) and (2) are satisfied with substantial margins. However, higher sodium volume fractions may be required to obtain a realistic thermalhydraulic design. Reducing the steel content also facilitates the problem of simultaneously satisfying conditions (1) and (2).

With incentive for reducing sodium and also steel content, both for economy (higher conversion ratios) and safety considerations, it is interesting to optimize for safety the 30% sodium volume fraction cases with a fuel-to-steel ratio of 2.0 (which is quite reasonable from a thermal, hydraulic and mechanical standpoint). Figure 5 shows $(\Delta k)_{Sod}$, $(\Delta k)_{Rod}$, and $\left[-(\Delta k)_{Dop}/2\right]+1$ versus core size for 30% sodium volume. The optimum core size, a 1.5 ft slab (or 2.3 x 4.6 ft at $L/D = \frac{1}{2}$), is at the crossover of the $(\Delta k)_{Sod}$ and $(\Delta k)_{Rod}$ curves and best satisfies safety criteria (1) and (2). The overall temperature coefficient $(dk/dT)_{Total}$ is -6.65×10^{-6} for this case.

The fuel slump reactivity effect can be rendered controllable by utilizing high density oxide in a core with a fairly low neutron leakage, and minimizing the L/D ratio. The low L/D ratio is also the direction that permits minimum sodium volume fraction, which is preferred for fuel economy and other safety considerations.

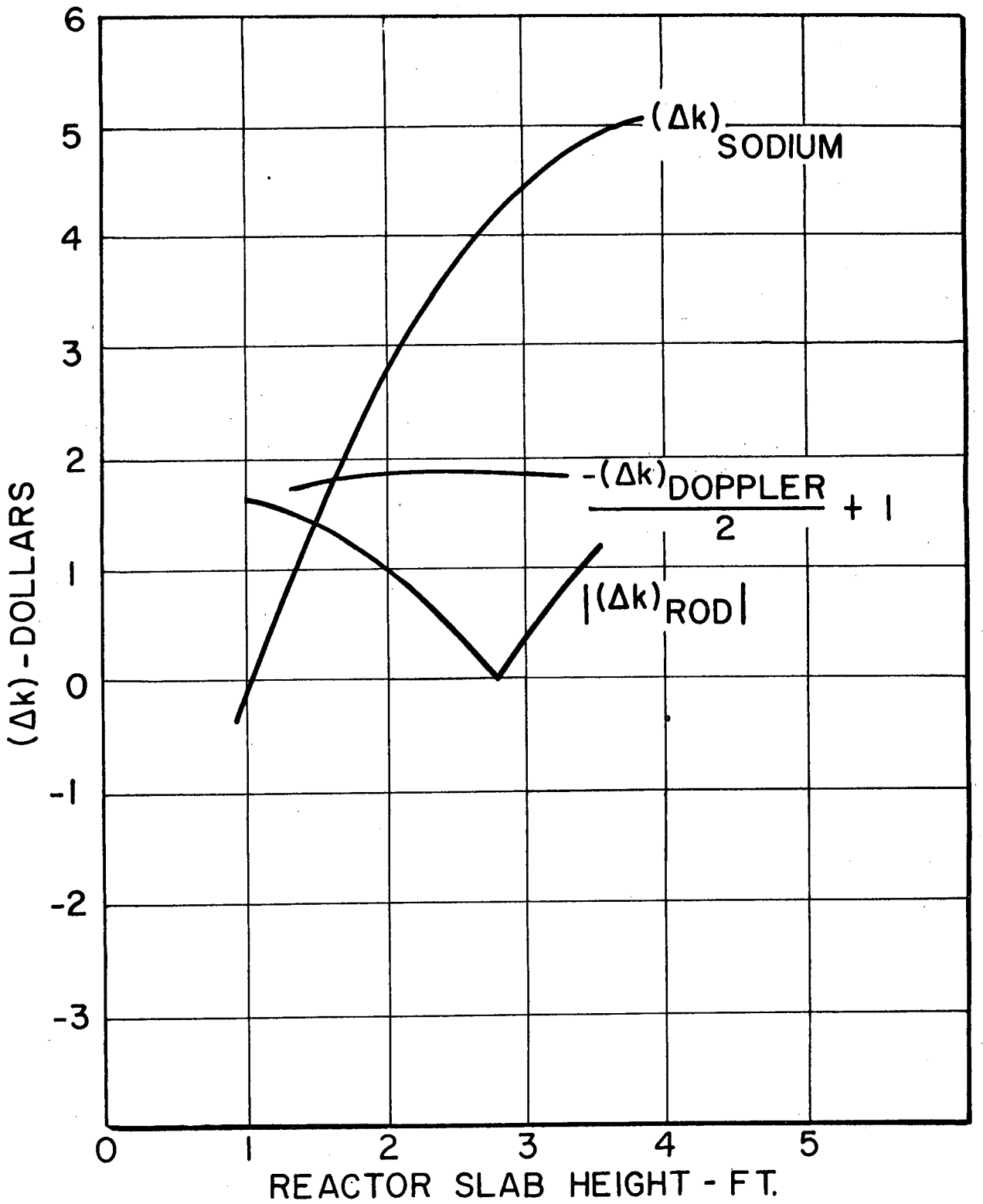

Figure 5 - Change in Reactivity Due to Total Doppler Available, Total Sodium Loss, and Loss of Control Rods for Blanketed Core Containing 30% Sodium.

APPENDIX I

EFFECT OF A BERYLLIUM REFLECTOR ON NEUTRON LIFETIME

A beryllium reflector was placed between the core and radial blanket for one typical design case in order to determine the resulting increase of the average neutron lifetime. It was expected that the beryllium would not appreciably affect other safety parameters. The case studied was a cylindrical reactor with both length and radius of 3.2 feet, the same composition and leakage as a 2 foot slab reactor with 30% sodium, and a fuel-to-steel ratio of 2 to 1. The beryllium reflector was 4 inches thick and was placed between the core and the first region of the radial blanket.

For this large fast oxide reactor, the prompt neutron lifetime increased only from 6.6×10^{-7} seconds to 11.6×10^{-7} seconds when the radial beryllium reflector was inserted. This factor of 1.8 is not a great enough improvement in the safety characteristics to warrant the increased cost and design complexity.

APPENDIX II

PU-239 RESONANCE INTEGRAL EVALUATION

The evaluation of the resonance integral for fissile material is more complex than for non-fissile material since both capture and fission resonances must be evaluated. The absorption resonance integral for Pu-239 was calculated using the relationship applicable to a homogeneous reactor,

$$I_{eff} = \int_{-\infty}^{\infty} \frac{\sigma_a \sigma_p}{\sigma_t} \frac{dE}{E} \qquad (II1)$$

where σ_a is the absorption cross section, σ_p is the potential scattering cross section per Pu-239 atom, σ_t is the total cross section, and E is energy. The RES Code[6] used to evaluate the above integral assumes that the energy dependence of the cross sections are given by the usual Doppler broadened, Breit-Wigner line shape.

In order to evaluate I_{eff} for Pu-239, Γ_γ was replaced by $\Gamma_a = \Gamma_f + \Gamma_\gamma$ where Γ_γ is the radiative capture width and Γ_f is the fission width. This calculation did not present any problem in the resolved resonance region, which for Pu-239 extends only up to 60 ev. For the unresolved resonance region, between 60 ev and 9000 ev, it was necessary to use a statistical distribution for both the neutron and fission widths based upon the analysis of Porter and Thomas[4]. The chi squared distribution function was used, given by

$$p(x,\rho)\,dx = \Gamma(\rho)^{-1}\,(\rho x)^{\rho-1}\,e^{-\rho x}\,dx \qquad (II2)$$

For numerical computations the neutron and fission width distributions were approximated by discrete widths, each representing a given fraction of the total distribution. Four widths used to represent the distribution of neutron widths

$$x_n = \Gamma_n^o / \langle \Gamma_n^o \rangle$$

were those values, $\bar{x}_n^i$ for i = 1, 2, 3 & 4, corresponding to

$$\int_o^x P\,(x,\tfrac{1}{2})dx = 1/8,\ 3/8,\ 5/8\ \&\ 7/8 \qquad (II3)$$

but normalized to give

$$\sum_{i=1}^{4} \bar{x}_n^i = 4$$

Only three representative values were used for the narrower fission width distribution ($\rho = 3/2$, as recommended by Bethe[8]) of $x_f = \Gamma_f / \langle \Gamma_f \rangle$. These were the values, $\bar{x}_f^k$ for k = 1, 2, 3, corresponding to

$$\int_o^x P(x,3/2)dx = 1/6,\ 3/6,\ \&\ 5/6 \qquad (II4)$$

but normalized to give $\sum_{k=1}^{3} \bar{x}_f^k = 3$

The average fission width was calculated as

$$\langle \Gamma_f \rangle = \Gamma_\gamma / \alpha(E) \qquad (II5)$$

where $\Gamma_\gamma = .039$ ev for the unresolved resonances and $\alpha(E)$, the ratio of capture-to-fission cross sections, was obtained as a function of energy from the best estimate based upon the available experimental data. Table VIII shows $\alpha(E)$ values for each of the 18-energy groups used in these calculations.

Table IX shows normalized values of $\bar{x}_n^i$ and $\bar{x}_f^k$, $\langle \Gamma_n^o \rangle$ and Γ_γ, and the corresponding values of Γ_n, Γ_f and $\Gamma_a = \Gamma_f + \Gamma_\gamma$ used in the Breit-Wigner form for one energy value (550 ev). The combination of four $\bar{x}_n^i$'s and three $\bar{x}_f^k$'s yields a statistical distribution of 12 equally probable resonance absorption integrals for each resonance. The resonance absorption strength for each energy group was computed as the average of the 12 single resonance integrals at the mean lethargy of the group. A resonance absorption strength was also computed for each group for the case of Pu-239 at infinite dilution (σ_p large). The ratio of these resonance absorption strengths gives the Pu-239 resonance self-shielding factor for each group. The infinite dilution fission cross section for each group was obtained by lethargy averaging the fission cross section curves in BNL-325[5]. Multiplying this value by the group self-shielding factor yielded the effective Pu-239 fission cross section. The radiative capture cross sections were then computed using the effective fission cross sections and the $\alpha(E)$ values listed in Table VIII.

TABLE VIII

Eighteen Group Values of $\alpha(E)$ for Pu-239

Group, j	$\bar{u}$	Ej(ev)	$\alpha(E)$[a]
1	.75	4.8×10^6	.02
2	1.75	1.77×10^6	.04
3	2.25	1.05×10^6	.05
4	2.75	$.65 \times 10^6$	.07
5	3.25	$.40 \times 10^6$	.10
6	3.75	$.28 \times 10^6$	.16
7	4.25	1.45×10^5	.23
8	4.75	$.88 \times 10^5$	.30
9	5.50	$.41 \times 10^5$	.37
10	6.50	$.15 \times 10^5$	.47
11	7.4	6.2×10^3	.52
12	8.5	2.0×10^3	.56
13	9.75	550	.62
14	10.9	185	.65
15	11.8	76	1.24
16	13.6	12.6	.60
17	15.8	1.4	.41
18	---	~.2	.49

a The first 10 group $\alpha(E)$ values were taken from ANL-5800.[2] Groups 11 through 14, the unresolved resonance groups, were estimated from experimental values given in KAPL-1793.[16] These $\alpha(E)$ values are approximately the midpoint values over the experimental ranges of uncertainty. The $\alpha(E)$ values in groups 15 through 18 are according to resolved resonance parameters and thermal cross sections in BNL-325.[5]

TABLE IX

UNRESOLVED RESONANCE PARAMETERS FOR Pu-239

1. Γ_n^o Calculation

			For E_i = 550 ev	
i	$\bar{x}_n^i$	$\bar{\Gamma}_n^o$(ev)	Γ_n^o(ev)	Γ_n(ev)
1	.032	.000661	.000018	.000496
2	.279	.000661	.00016	.00432
3	.947	.000661	.00054	.0147
4	2.742	.000661	.00156	.0425

2. Γ_f and Γ_a Calculation

			For E_i = 550 ev	
k	$\bar{x}_f^k$	Γ_γ(ev)	Γ_f(ev)	$\Gamma_a=\Gamma_f+\Gamma_\gamma$
1	.310	.039	.0195	.0585
2	.854	.039	.0536	.0926
3	1.836	.039	.116	.155

APPENDIX III

CROSS SECTIONS FOR U-238, PU-239, PU-240, and FISSION PRODUCTS

Group No.	Δu	E_L ev	Isotope	σ_p (a)	300°K		750°K		1500°K		2500°K	
					σ_f	σ_c	σ_f	σ_c	σ_f	σ_c	σ_f	σ_c
1	1.5	2.25×10^6	U-238	40	.590	.015	.590	.015	.590	.015	.590	.015
2	0.5	1.35×10^6			.450	.062	.450	.062	.450	.062	.450	.062
3	0.5	8.25×10^5			.003	.130	.003	.130	.003	.130	.003	.130
4	0.5	5.0×10^5			0	.143	0	.143	0	.143	0	.143
5	0.5	3.0×10^5				.130		.130		.130		.130
6	0.5	1.8×10^5				.150		.150		.150		.150
7	0.5	1.1×10^5				.200		.200		.200		.200
8	0.5	6.7×10^4				.299		.300		.301		.301
9	1.0	2.5×10^4				.397		.400		.402		.403
10	1.0	9100				.601		.610		.615		.617
11	0.8	4000				.399		.440		.467		.487
12	1.4	1000				.728		.850		.940		1.02
13	1.2	300				.850		1.03		1.21		1.35
14	1.1	100				1.55		1.80		2.07		2.36
15	1.2	30				2.31		2.48		2.69		2.91
16	1.8	5				4.02		4.14		4.32		4.52
17	2.5	0.4				0.40		0.40		0.40		0.40
18	---	0				1.52		1.52		1.52		1.52

(a) σ_p is the potential scattering cross section per isotopic fuel atom in barns. This was calculated for a reactor containing 40% sodium with a fuel to steel volume ratio of 2:1. The U-238 atom fraction in fuel was taken to be 0.9. The higher values of σ_p for Pu-239 and Pu-240 were calculated for atom fractions of .10 and .05, respectively, while the lower values were for atom fractions of 0.15 and 0.075.

Group No.	Isotope	σ_p	300°K σ_f	300°K σ_c	750°K σ_f	750°K σ_c	1500°K σ_f	1500°K σ_c	2500°K σ_f	2500°K σ_c
1	Pu-239	370	2.00	.040	2.00	.040	2.00	.040	2.00	.040
2			1.95	.078	1.95	.078	1.95	.078	1.95	.078
3			1.86	.093	1.86	.093	1.86	.093	1.86	.093
4			1.75	.123	1.75	.123	1.75	.123	1.75	.123
5			1.70	.170	1.70	.170	1.70	.170	1.70	.170
6			1.68	.269	1.68	.269	1.68	.269	1.68	.269
7			1.73	.398	1.73	.398	1.73	.398	1.73	.398
8			1.80	.540	1.80	.540	1.80	.540	1.80	.540
9			2.00	.740	2.00	.740	2.00	.740	2.00	.740
10			2.25	1.06	2.25	1.06	2.25	1.06	2.25	1.06
11			2.57	1.33	2.58	1.34	2.58	1.34	2.59	1.34
12			3.83	2.14	3.89	2.17	3.91	2.19	3.93	2.20
13			7.24	4.50	7.60	4.73	7.81	4.86	7.92	4.93
14			15.2	9.86	16.5	10.7	17.6	11.4	18.2	11.9
15			13.8	17.1	15.4	19.1	16.9	20.9	18.1	22.4
16			26.5	15.9	28.2	16.9	30.1	18.1	31.8	19.1
17			56.0	23.0	56.0	23.0	56.0	23.0	56.0	23.0
18	↓	↓	986.0	480.0	986.0	480.0	986.0	480.0	986.0	480.0
1	Pu-239	247	2.00	.040	2.00	040	2.00	.040	2.00	.040
2			1.95	.078	1.95	.078	1.95	.078	1.95	.078
3			1.86	.093	1.86	.093	1.86	.093	1.86	.093
4			1.75	.123	1.75	.123	1.75	.123	1.75	.123
5			1.70	.170	1.70	.170	1.70	:170	1.70	.170
6			1.68	.269	1.68	.269	1.68	.269	1.68	.269
7			1.73	.398	1.73	.398	1.73	.398	1.73	.398
8			1.80	.540	1.80	.540	1.80	.540	1.80	.540
9			2.00	.740	2.00	.740	2.00	.740	2.00	.740
10			2.25	1.06	2.25	1.06	2.25	1.06	2.25	1.06
11			2.55	1.32	2.56	1.33	2.57	1.33	2.58	1.34
12			3.73	2.09	3.82	2.13	3.86	2.16	3.88	2.17
13			6.76	4.21	7.21	4.46	7.49	4.66	7.65	4.76
14			13.4	8.73	14.9	9.68	16.0	10.4	16.9	11.0
15			11.7	14.5	13.1	16.3	14.5	18.0	15.7	19.5
16			22.5	13.5	23.9	14.4	25.6	15.3	27.1	16.3
17			56.0	23.0	56.0	23.0	56.0	23.0	56.0	23.0
18	↓	↓	986.0	480.0	986.0	480.0	986.0	480.0	986.0	480.0

Group No.	Isotope	σ_p	300°K σ_f	300°K σ_c	750°K σ_f	750°K σ_c	1500°K σ_f	1500°K σ_c	2500°K σ_f	2500°K σ_c
1	Pu-240	740	1.60	.020	1.60	.020	1.60	.020	1.60	.020
2			1.50	.080	1.50	.080	1.50	.080	1.50	.080
3			1.35	.180	1.35	.180	1.35	.180	1.35	.180
4			0.70	.200	0.70	.200	0.70	.200	0.70	.200
5			0.18	.200	0.18	.200	0.18	.200	0.18	.200
6			0.03	.200	0.03	.200	0.03	.200	0.03	.200
7			0	.300	0	.300	0	.300	0	.300
8				.450		.450		.450		.450
9				.700		.700		.700		.700
10				1.00		1.00		1.00	1.	1.00
11				1.15		1.17		1.18		1.19
12				2.98		3.10		3.17		3.22
13				6.88		7.50		7.96		8.28
14				15.9		18.3		20.5		22.1
15				16.6		19.4		22.2		24.3
16				4.62		5.43		6.17		6.76
17				193.0		193.0		193.0		193.0
18				208.0		208.0		208.0		208.0
1	Pu-240	494	1.60	.020	1.60	.020	1.60	.020	1.60	.020
2			1.50	.080	1.50	.080	1.50	.080	1.50	.080
3			1.35	.180	1.35	.180	1.35	.180	1.35	.180
4			0.70	.200	0.70	.200	0.70	.200	0.70	.200
5			0.18	.200	0.18	.200	0.18	.200	0.18	.200
6			0.03	.200	0.03	.200	0.03	.200	0.03	.200
7			0	.300	0	.300	0	.300	0	.300
8				.450		.450		.450		.450
9				.700		.700		.700		.700
10				1.00		1.00		1.00		1.00
11				1.13		1.15		1.16		1.17
12				2.82		2.97		3.07		3.13
13				6.10		6.77		7.29		7.67
14				13.1		15.3		17.3		18.8
15				13.4		15.7		18.0		19.9
16				3.73		4.43		5.10		5.66
17				158.0		158.0		158.0		158.0
18				208.0		208.0		208.0		208.0

Group No.	Isotope	σ_{tr}	σ_c
1	Fission Products	4.22	0.13
2		4.12	0.13
3		3.95	0.16
4		4.57	0.18
5		6.18	0.19
6		7.20	0.21
7		8.82	0.24
8		10.85	0.27
9		13.89	0.34
10		8.53	0.55
11		16.8	0.80
12		16.2	2.2
13		28.5	5.5
14		35.6	12.6
15		43.0	20.0
16		79.0	56.0
17		53.0	30.0
18		73.0	50.0

APPENDIX IV

EVALUATION OF DOPPLER EFFECTS WITH SPATIAL TEMPERATURE AND POWER DISTRIBUTIONS

The Doppler coefficient for spatially uniform flux and fuel temperature is given by

$$(dk/dT) = \Delta k/\Delta \bar{T} = \frac{k_2 - k_1}{\bar{T}_2 - \bar{T}_1} \qquad \text{(IV1)}$$

where $\Delta \bar{T}$ is the temperature change in the average fuel.

The Doppler coefficient is of practical interest as a reactor power coefficient. Consequently, the effective Doppler coefficient must take into account the following space dependent effects: (1) neutron flux and importance, (2) gross fuel temperature distribution over the reactor and radially across an individual fuel rod, and (3) the fuel temperature response to a change of reactor power. Assuming a 1/T dependence of the Doppler coefficient on absolute temperature, T, the effective Doppler temperature coefficient was obtained from the uniform coefficient, $dk/d\bar{T}$, using the relationship:

$$C_1 = \frac{(dk/d\bar{T})_{eff}}{(dk/d\bar{T})} = \frac{\bar{C}_2 \bar{T} \int_o^{R_{max}} \int_o^{Z_{max}} \left[P(R,Z)\right]^2 \frac{dT(R,Z)}{d\bar{T}} \frac{RdRdZ}{T(R,Z)}}{\int_o^{R_{max}} \int_o^{Z_{max}} \left[P(R,Z)\right]^2 RdRdZ} \qquad \text{(IV2)}$$

where $\bar{C}_2$ is a correction factor for the parabolic radial temperature distribution across an individual fuel rod, $\bar{T}$ is the average fuel temperature in °K, and T(R,Z) and P(R,Z) are the fuel temperature and relative power density at core coordinates R and Z. These two functions were approximated by

$$T(R,Z) = T_o + P(R,Z)(\bar{T} - T_o)$$

with T_o taken as the average coolant temperature, and

$$P(R,Z) = P_R P_Z \left[1 - 2\left(1 - \frac{1}{P_R}\right)\left(\frac{R}{R_{max}}\right)^2\right]\left[1 - 3\left(1 - \frac{1}{P_Z}\right)\left(\frac{Z}{Z_{max}}\right)^2\right]$$

where P_R and P_Z are respectively the peak-to-average radial and axial core power densities. Equation (IV2) uses the square of the power distribution as an approximation of the product of the neutron flux and importance.

The correction factor $\bar{C}_2$ was obtained using the relationship

$$\bar{C}_2 = \frac{\int_o^{R_{max}} \int_o^{Z_{max}} \left[P(R,Z)\right]^2 C_2(R,Z)\, RdRdZ}{\int_o^{R_{max}} \int_o^{Z_{max}} \left[P(R,Z)\right]^2 RdRdZ} \qquad \text{(IV3)}$$

where

$$C_2(R,Z) = \left(\frac{T_c+T_o}{2}\right)(2/r_{max}^2)\int_o^{r_{max}} \frac{rdr}{T(r)} = \frac{1}{2}\left[\frac{\frac{T_c}{T_o}+1}{\frac{T_c}{T_o}-1}\right] \log_e\left(\frac{T_c}{T_o}\right)$$

and r is the radial coordinate for an individual fuel rod, T_c is the central fuel rod temperature at the core coordinates (R,Z), $^cT(r)$ is the temperature across the fuel rod, given by

$$T(r) = T_c - (T_c-T_o)\,(r/r_{max})^2$$

In order to simplify the evaluation of the integral in the numerator of equation (IV3), $C_2(R,Z)$ was fitted to the following linear expression in the ratio T_c/T_o:

$$C_2(R,Z) = 0.95 + 0.05\; T_c(R,Z)/T_o$$

The linear fit is adequate since C_2 does not depart appreciably from unity over the range of $T_c(R,Z)$ values in the core. The distribution of center fuel rod temperatures over the core is given by

$$T_c(R,Z) = T_o + P(R,Z)\,(\bar{T}_c - T_o)$$

where $\bar{T}_c$ is the central fuel temperature at the point of average core power density.

For the scoping study covered in this document, the following values were assumed: P_R=1.6; P_Z=1.25; T_o=725°K; $\bar{T}$=1170°K; and $\bar{T}_c$=1400°K. These yielded $\bar{C}_2$=1.08 from equation (IV3); and C_1=1.23 from equation (IV2) for the overall correction factor on the uniform-temperature Doppler coefficient.

Similar corrections for spatially non-uniform temperature distributions can be made for the total Doppler reactivity reduction $(\Delta k)_{Dop}$ in a power excursion. Again assuming a 1/T fuel temperature dependence for the Doppler coefficient, this correction factor is given by

$$C_3 = \frac{\left[(\Delta k)_{Dop}\right]_{eff}}{\left[(\Delta k)_{Dop}\right]_{\bar{T}}} = \frac{\bar{C}_4}{\log_e \frac{\bar{T}_2}{\bar{T}_1}} \cdot \frac{\int_o^{R_{max}}\int_o^{Z_{max}} \left[P(R,Z)\right]^2 \left[\log_e \frac{T_2(R,Z)}{T_1(R,Z)}\right] RdRdZ}{\int_o^{R_{max}}\int_o^{Z_{max}} \left[P(R,Z)\right]^2 RdRdZ} \qquad \text{(IV4)}$$

where $T_1(R,Z)$ and $T_2(R,Z)$ are the average fuel temperatures in the rod at core coordinate (R,Z) respectively before and after the excursion. These functions can be expressed in terms of average temperatures as follows:

$$T_1(R,Z) = T_o + P(R,Z)\,(\bar{T} - T_o)$$

$$T_2(R,Z) = T_1(R,Z) + P(R,Z)\,(\bar{T}_2 - \bar{T}_1)$$

where $\overline{T}_1$ and $\overline{T}_2$ are core-averaged fuel temperatures respectively before and after the excursion.

The correction factor $\overline{C}_4$ takes into account the non-uniform temperature distribution across an individual fuel rod and is given by

$$\overline{C}_4 = \frac{\int_0^{R_{max}} \int_0^{Z_{max}} \left[P(R,Z)\right]^2 C_4(R,Z)\, RdRdZ}{\int_0^{R_{max}} \int_0^{Z_{max}} \left[P(R,Z)\right]^2 RdRdZ} \qquad \text{(IV5)}$$

where

$$C_4(R,Z) = \left(2 \Big/ \log_e \frac{\overline{T_2(r)}}{\overline{T_1(r)}}\right) \int_0^{r_{max}} \log_e \frac{T_2(r)}{T_1(r)}\, rdr$$

The radial temperature distribution $T_1(r)$, is given by a parabola

$$T_1(r) = T_c(R,Z) - \left[T_c(R,Z) - T_o\right](r/r_{max})^2$$

while

$$T_2(r) = T_1(r) + P(R,Z)\,(\overline{T}_2 - \overline{T}_1),$$

$$\overline{T_1(r)} = \tfrac{1}{2}\left[T_c(R,Z) + T_o\right]$$

and $\overline{T_2(r)} = \overline{T_1(r)} + P(R,Z)\,(\overline{T}_2 - \overline{T}_1)$

The correction factor, C_3, was evaluated for a power excursion occuring at full power operation using the following values: P_R=1.6; P_Z=1.25; T_o=725°K; $\overline{T}_1$=1170°K; $\overline{T}_c$=1420°K; and $\overline{T}_2$=2260°K.

These values yielded $\overline{C}_4$ = 1.037 and C_3 = 1.09 for the overall correction factor to be applied to uniform temperature $(\Delta k)_{Dop}$.

For a power excursion from a cold reactor, the values were taken to be: P_R=1.6; P_Z=1.25; $T_o = \overline{T} = \overline{T}_1 = \overline{T}_c$ = 273°K; T_2 = 2020°K, which gave correction factors of $\overline{C}_4$ = 1.0 and C_3 = 1.09.

The values for $\overline{T}_2$ were computed by assuming that just enough fission energy could be generated in the fuel rod at the reactor center (position of peak power density) to bring this fuel to its melting temperature, ~3023°K, and melt it. Since the heat of fusion is 750 times the specific heat of the fuel, the average fuel would have an additional increase in temperature of 375°K (for peak-to-average power density=2) during the time that the peak fuel was undergoing the phase change at its melting temperature. In numerically evaluating the integrals in equations (IV4) and (IV5), values of $T_2(R,Z)$ which were above 3023°k were set at 3023°K before integrating.

APPENDIX V

SIMPLIFIED KINETICS MODEL TO EVALUATE SAFETY CRITERIA FOR REACTIVITY COEFFICIENTS

Consider a step reactivity increase, $(\Delta k)_{step}$ (more than \$1), at time t=0, and a constant (temperature independent) prompt temperature coefficient approximated by $-(\Delta k)_{Dop}/(\Delta T)_{max}$, where $(\Delta T)_{max}$ is the maximum allowable fuel temperature rise above the normal operating condition. For calculational convenience the spacial fuel temperature distribution is neglected, but the Doppler reactivity decrease $(\Delta k)_{Dop}$ has been reduced to account for the non-uniform power and fuel temperature distribution, assuming a 1/T variation of the Doppler coefficient (see footnote under Table III).

The kinetics equations under these prompt critical conditions is approximated by

$$\frac{dP}{dt} = \frac{(\rho-1)\beta}{\ell} P \qquad (V1)$$

$$\rho = (\Delta k)_{step} + \left[\frac{(\Delta k)_{Dop}/(\Delta T)_{max}}{C_f}\right]\int_o^t (P - Po)dt \qquad (V2)$$

assuming the heat loss from the fuel during a prompt excursion will remain at the normal operating level. In equations (V1) and V2) the following definitions apply:

P = fuel power density

P_o = normal operating power density

ρ = reactivity in dollar units

β = effective delayed neutron fraction

ℓ = average prompt neutron lifetime

t = time

C_f = heat capacity per unit volume of fuel

Differentiating equation (V2) with respect to time and dividing by dP/dt gives a reactivity - power change relationship. Then integrating with respect to P gives

$$C_f\left[\frac{(\Delta k)_{step} - \rho}{(\Delta k)_{Dop}/(\Delta T)_{max}}\right]\left[\frac{(\Delta k)_{step} + \rho - 2}{2\ell}\right]\beta = -P_o\left[\left(\frac{P}{P_o}\right) - \left(1 + \log\frac{P}{P_o}\right)\right] \qquad (V3)$$

When $t = 0$, $\rho = (\Delta k)_{step}$ and $P = P_o$. The power excursion is terminated when P returns to P_o, corresponding to $\rho = 2 - (\Delta k)_{step}$. The fuel temperature rise is then

$$(\Delta T) = \int_o^t \frac{P - P_o}{C_f}\, dt = \frac{-2\left[(\Delta k)_{step} - 1\right]}{(\Delta k)_{Dop}/(\Delta T)_{max}} \qquad (V\,4)$$

from equation (V 2). The required condition is that (ΔT) be less than $(\Delta T)_{max}$. This is satisfied if

$$\frac{-(\Delta k)_{Dop}}{2} + 1 > (\Delta k)_{step} \qquad (V\,5)$$

Substituting $(\Delta k)_{step} = (\Delta k)_{sod}$ and $(\Delta k)_{step} = (\Delta k)_{rod}$ yields the prescribed safety conditions in Section V.

VI REFERENCES

1. F. W. Thalgott, et al, "Stability Studies on EBR-1", A/Conf. 15, P/1845 (1958).

2. ANL-5800, Reactor Physics Constants, July 1, 1958.

3. J. L. Rosen, "Neutron Resonances in U-238" (Thesis), CU-185, (1959).

4. C. E. Porter and R. G. Thomas, "Fluctuations of Nuclear Reaction Widths", Physical Review, 104, p/483-91 (1956).

5. D. J. Hughes and R. B. Schwartz, Neutron Cross Sections, BNL-325, July, 1958.

6. F. T. Adler, G. W. Hinman and L. W. Nordheim, The Quantitative Evaluation of Resonance Integrals, GA-350, A/Conf. 15, P/1988, Sept.,1958.

7. L. Dresner. "The Effective Resonance Integrals of U-238 and Th-232", Nuclear Science and Engineering, 1, 1:68-79, (1956).

8. H. A. Bethe, On the Doppler Effect in Fast Reactors, APDA-119, March 1957.

9. H. Feshbach, G. Goertzel and H. Yamauchi, "Estimation of Doppler Effect in Fast Reactors", Nuclear Science and Engineering, 1, 1:4-20, (1956).

10. Report on HEDO Computer Code to be released soon.

11. P. Aline, P. Greebler, and J. Sueoka, Fast Oxide Breeder-Reactor Physics, Part I - Parametric Study of 300(e) MW Reactor Core, GEAP-3287, Nov., 1959.

12. APDA-124, Enrico Fermi Atomic Power Plant, January, 1959.

13. R. B. Nicholson, "The Doppler Effect in Fast Neutron Reactors", Transactions of the American Nuclear Society, 1960 Winter Meeting, December 12-15, 1960, P/364.

14. D. K. Butler, R. T. Frost, and W. Y. Kato, "Measurements of Doppler Temperature Coefficients in Intermediate and Fast Assemblies", A/Conf. 15, P/1777, (1958).

15. J. B. Nims and P. F. Zweifel, Preliminary Report on Sodium Temperature Coefficients in Large Fast Reactors, APDA-159, (1959).

16. D. B. Molino and J. B. Simpson, An $\alpha_{49}(E)$ Curve Consistent with EBR-1 Measurements and also with Most Former Measurements, KAPL-1793, May, 1957.

17. R. Avery, "Coupled Fast-Thermal Power Breeder", Nuclear Science and Engineering, 3, 2:129-144, (1958).